Synthetic Routes to the Encapsulation of II–VI Semiconductors in Mesoporous Hosts

Elizabeth A. Turner,[a] Yining Huang,*[a] and John F. Corrigan*[a]

Keywords: Mesoporous materials / Semiconductors / Host–guest systems / Nanostructures

Ordered mesoporous silicate materials, such as MCM-41 and SBA-15, offer a nanometre-sized environment for the inclusion of quantum-confined materials. The channel walls of the framework hinder cluster-cluster interactions thereby restricting particle growth and thus limiting the size of the enclosed particles to the nanometre-size regime. In particular, the past decade has seen substantial progress in the synthesis and encapsulation of II–VI nanoparticles within MCM-41 and SBA-15. This microreview highlights the recent developments in this area, with notable emphasis on the synthetic routes used in the growth and anchoring of CdS, CdSe and ZnS nanoparticles within a mesoporous host. Of relevance are the methods of ion-exchange, interior pore wall modification, quantum-dot doping, incorporation of preformed nanoparticles and clusters and external surface passivation through organic functionalization. In addition to synthetic methods employed, the interesting photochemical properties of the composite materials are discussed.

Introduction

Ordered porous silicate materials have been the subject of intense investigation over the past several decades.[1] These materials are generally categorized according to pore size, corresponding to the spherical diameter of the aperture. IUPAC has defined three classifications of porous materials which include microporous (< 2 nm in diameter), mesoporous (2–50 nm) and macroporous (> 50 nm).[2] Although microporous materials have been successfully used in the formation of inorganic–organic hybrid materials, the advent of the first ordered mesoporous materials[3] marked a pivotal moment in the advancement of host–guest chemistry.

Since the development of MCM-41 (**M**obil's **c**omposition of **m**atter) in the early nineties[3] and the subsequent discovery of SBA-15 (**S**anta **B**arbar**a**) in 1998,[4] a considerable amount of work has focused on understanding both the mechanistic formation[5] and characterization[6] of these intriguing silicate/aluminosilicate materials. Recognizing that

[a] Department of Chemistry, The University of Western Ontario, London, Ontario, N6A 5B7, Canada
Fax: +1-519-661-3022
E-mail: yhuang@uwo.ca
jfcorrig@uwo.ca

Elizabeth A. Turner (centre) was born in Halifax, Nova Scotia, Canada in 1980. She obtained her B. Sc. (Honours) from Saint Mary's University in Halifax, Nova Scotia in 2002. She is currently pursuing her Ph. D. at The University of Western Ontario in London, Ontario under the supervision of Dr. John F. Corrigan and Dr. Yining Huang. Her research interests are in the synthesis and characterization of ternary metal–metal chalcogenides in mesoporous materials and the development of new binary chalcogenide reagents. Yining Huang (right) was born in Beijing, P. R. China. He earned his B.Sc., M.Sc. from Peking University and his Ph. D. from McGill University with Ian S. Butler and Denis F. R. Gilson. He was a NSERC post-doctoral fellow with Colin A. Fyfe at the University of British Colombia. He started his academic career at Laurentian University as an Assistant Professor in 1995 and then moved to The University of Western Ontario in 1997 where he is currently Professor of Chemistry. His major research interests include characterization of nanoporous materials and the host–guest interactions in these systems. John F. Corrigan (left) was born in Oshawa, Ontario, Canada. He obtained his B.Sc. (Chemistry Specialist) from the University of Toronto in 1990 and his Ph. D. degree from the University of Waterloo in 1995 with Arthur J. Carty. After a NSERC post-doctoral fellowship at the University of Karlsruhe with Dieter Fenske, he joined the faculty at The University of Western Ontario in 1997 where he is currently an Associate Professor. His current research interests focus on metal chalcogenolate and chalcogenide complexes, from coordination complexes to nanomaterials.

MICROREVIEWS: This feature introduces the readers to the authors' research through a concise overview of the selected topic. Reference to important work from others in the field is included.

the distinctive hexagonal array of uniform mesoporous channels can be used in inclusion chemistry,[7] the past decade has seen an explosion of growth in the use of mesoporous materials as a host environment for catalysis,[8] adsorption/separation,[9] polymerization,[10] and in particular, the subject of this microreview, quantum-confined materials.

The original synthesis for purely siliceous MCM-41 is done under acidic conditions with the use of alkyltrimethylammonium halide as an organic structure directing agent and sodium silicate as a silica source.[3] A liquid-crystal templating method (Figure 1) has been proposed for the formation of MCM-41, where surfactant species form micellar rods in aqueous solution which can align in a hexagonal array.[3,5] The addition of an anionic inorganic species into the aqueous domain initiates the formation of inorganic walls between the surfactant micelles in an effort to balance the cationic charge of the hydrophilic micelle. Increasing the alkyl chain length of the surfactant and the use of an organic auxiliary swelling agent (e.g. 1,3,5-trimethylbenzene) have been found to result in pore-size expansion, further supporting the proposed liquid-crystal templating mechanism. The porous silica skeleton is obtained through calcination of the surfactant-silica material at 540 °C, thus removing all organic components from the interior pore.

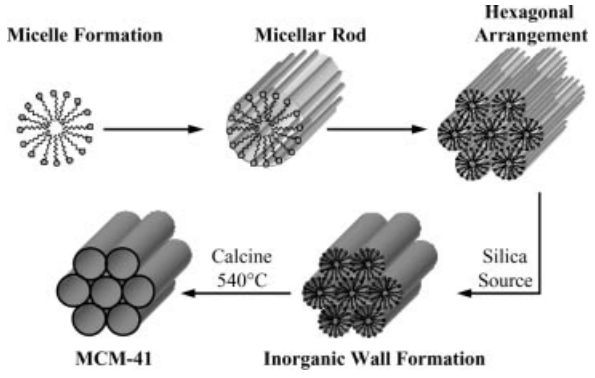

Figure 1. Proposed liquid-crystal templating method for the formation of mesoporous MCM-41.

Although the pore size of MCM-41 can range from 1.6–10 nm, the larger pore systems generally show decreased regularity of the hexagonal array as observed by transmission electron microscopy (TEM), Figure 2, a–b. In addition, the thin walls of MCM-41 (1–1.5 nm) are not strong enough to retain the framework structure upon hydrothermal treatment. The pore walls can be strengthened using a secondary crystallization technique,[11] modified reaction conditions[12] and post-synthesis restructuring.[13] These approaches, however, result in a pore-wall thickness having an upper limit of ca. 3 nm. On the other hand, SBA-15[4] is a thicker-walled mesoporous material (3.1–6.4 nm) with pore sizes spanning 4.7–30 nm. Although SBA-15 has a similar hexagonal arrangement of mesoporous channels to MCM-41, the material is formed from a nonionic triblock copolymer of poly(ethylene oxide)–poly(propylene oxide)–poly(ethylene oxide). Pore-size engineering can be accomplished by adjusting the reaction temperature (35–140 °C) and time (11–74 h), as well as by altering copolymer composition or through the addition of an organic swelling agent. The increased pore thickness enables SBA-15 to exhibit greater hydrothermal stability as compared to its MCM-41 counterpart. Furthermore, SBA-15 displays increased regularity in pore size uniformity as is shown in Figure 2c–d.

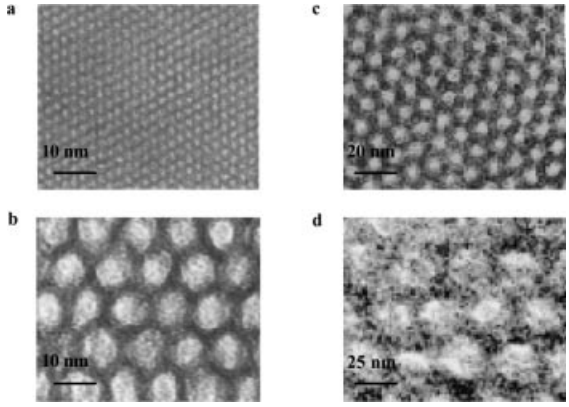

Figure 2. Transmission electron microscope images of MCM-41: Pore size a) 2 nm, b) 10 nm and SBA-15: Pore size c) 6 nm, d) 26 nm. (Figure 1, a–b, adapted with permission from ref.[3b]. Copyright 1992, American Chemical Society. Figure 1, c–d, reprinted and modified with permission from ref.[4a]; D. Zhao, J. Feng, Q. Huo, N. Melosh, G. H. Fredrickson, B. F. Chmelka, G. D. Stucky, Science 1998, 279, 548–552. Copyright 1998, AAAS).

One of the many attractive features of MCM-41 and SBA-15 is the relatively high surface area offered by the mesoporous framework, typically ranging between 700 and 1000 $m^2 g^{-1}$, thus rendering these surfaces available for guest molecule inclusion. Upon occupying the host with a guest species a notable decrease in surface area is observed. Nitrogen adsorption is the most commonly used technique to monitor changes in pore size, surface area and pore volume.[14] Type-IV isotherms[2] are observed for both MCM-41 and SBA-15 and are marked with a sharp inflection point at a value P/P_0, corresponding to capillary condensation within the primary mesopores (Figure 3). The surface area is calculated based on the Brunauer–Emmett–Teller (BET) method,[15] where a decrease in BET surface area is characterized by a decrease in the P/P_0 position for capillary condensation. The results from nitrogen adsorption can also be used in the calculation of pore size distribution based on the Barrett–Joyner–Halenda (BJH) method.[16] It is important to note, however, that the BJH calculation tends to underestimate the pore size by approximately 1 nm for pore dimensions less than 4 nm.[17] Nonetheless, the trend in decreasing pore size as a result of pore filling can be monitored using this calculation.

Upon enclosing guest molecules within the host material it is essential that the siliceous framework remains intact both during and after inclusion of the desired species. The hexagonal array is unambiguously monitored by TEM, however, powder X-ray diffraction (PXRD) is another useful tool in surveying the framework structure. MCM-41 displays a very strong d_{100} spacing at low angle with slightly weaker reflections corresponding to lattice planes (110) and

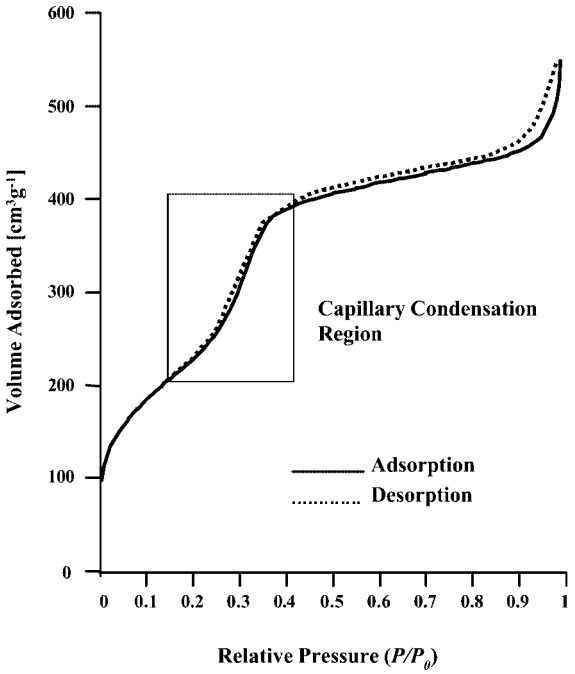

Figure 3. Typical type-IV isotherm observed for mesoporous materials. Depicted is the adsorption–desorption isotherm for calcined MCM-41.

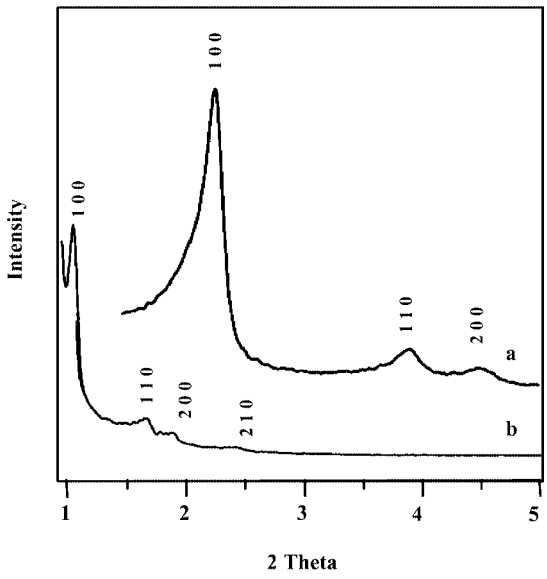

Figure 4. Powder X-ray diffraction patterns for a) MCM-41 and b) SBA-15. (Figure adapted with permission from ref.[42]. Copyright 2002, American Chemical Society).

(200) at higher angle, as seen in Figure 4 (a).[3] Similarly, SBA-15 displays a predominant d_{100} spacing with three additional well-resolved peaks related to the (110), (200) and (210) lattice planes at higher angles (Figure 4, b).[4] Retention of these peaks upon guest-molecule inclusion is indicative of framework stability. Typical pore filling is accompanied by a reduction in peak intensity of the composite material in the corresponding PXRD pattern. This results from a decrease in scattering contrast between the pores and the walls of the mesoporous material upon pore filling. In addition, the position of the d_{100} peak is often shifted to lower angles as pore size decreases.

The field of quantum-confined nanocrystals has grown tremendously with the discovery of the size-dependent chemical, electronic and physical properties of semiconductor materials.[18] Conventional semiconductors are characterized by a filled valence band and empty conduction band separated by a discrete bandgap energy. The progression to smaller-sized particles (smaller than the Bohr radius[19]) having the same chemical composition as that of the bulk material results in an increase in bandgap energy, coupled with the quantization of both the valence and conduction bands (Figure 5). Upon entering this nanometre size regime, the Bohr radius of the exciton exceeds the size of the particle itself and thus, the exciton "fits" into the given particle by adopting a higher kinetic energy. As such, an increase in bandgap energy is observed as a result of quantum-confinement effects. These effects are readily monitored using UV/Vis absorption spectroscopy where shifts to higher energy with decreasing size vs. the bulk material are observed. Thus UV/Visible spectroscopy can be used to demonstrate the effects of quantum confinement in II–VI particles of various sizes, highlighted by the systematic shift of the excitonic transition to higher energy with decreasing particle size. These materials are composed of metal atoms from group 12 (Zn, Cd, Hg) and chalcogen atoms from group 16 (S, Se, Te). Hence, a blue shift in absorbance onset from that of the bulk material is observed.[18c] The photoluminescence (PL) of II–VI nanoparticles occurs as two types; band-edge PL and deep-trap PL. Band-edge emission occurs due to the recombination of trapped charge carriers from shallow trap states within the particle, and this results in a slight red shift with respect to the absorption due to the relaxation of the trapped charge carrier into lower lying energy states prior to recombination. Deep-trap emission occurs through recombination of trapped localized carriers from deep mid-gap trap states, which are usually hole traps at the surface of the particle. Trapped emission is characterized by a broad line width which is shifted significantly to the red of the excitonic absorption.[18,19]

One of the challenges in obtaining monodisperse nanoparticles is in controlling their growth and thus preventing their aggregation to the bulk state. In particular, there has been substantial interest in developing suitable chemical capping agents for these nanometre-sized particles. Recent efforts have focused on the use of polymers,[20] organic ligands[21] and inorganic functionalization in core/shell materials[22] to passivate the nanoparticle surface, although particle size distribution is inevitable within these systems. An alternative method potentially leading to monodisperse or nearly monodisperse particles is through the use of an ordered mesoporous host such as MCM-41 and SBA-15. The pore-size structure of these materials is ideal for the growth of nanoparticle semiconductor materials, where the confining nanosized environment hinders particle–particle interactions thus preventing cluster aggregation.

Perhaps the most extensively studied class of semiconductor materials is that referred to as the II–VI semi-

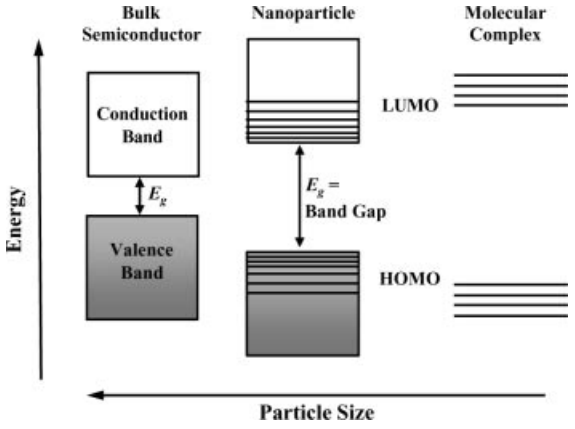

Figure 5. Energy diagram depicting the relationship between particle size and bandgap for a bulk semiconductor, nanoparticle and molecular species.

conductors. Two polymorphs of these metal chalcogenide materials are known, referred to as zinc blende (or sphalerite) and wurtzite, where both M^{2+} (M = Zn, Cd, Hg) and E^{2-} (E = S, Se, Te) are tetrahedrally coordinated.[23] Zinc blende can be represented as two interpenetrating face-centred cubic lattices, where the anion occupies one cubic lattice in which a quarter of the tetrahedral holes are populated by the cation of a second cubic lattice. In contrast, the wurtzite structure has hexagonal symmetry where anions form a hexagonal closest-packed arrangement in which half of the tetrahedral holes are occupied by metal atoms of a second hexagonal closest-packed array. For some metal chalcogenides both polymorphs are observed where one form is thermodynamically favoured over the other.[24] For metal sulfides, both forms occur naturally, however, zinc blende is more stable for ZnS, whereas the thermodynamically favoured wurtzite structure is observed for CdS. In comparison, both structures are observed in the case of CdSe (preferentially wurtzite), while ZnSe is only found in the zinc blende form. The reverse is true for metal tellurides, where CdTe is found only as a zinc blende structure, while for ZnTe the zinc blende form is preferred but it also displays the wurtzite structure.

It is the intention of this microreview to discuss the various synthetic strategies employed in the formation of II–VI materials within a mesoporous host with emphasis on the quantum-confinement effects observed within these composite materials.

Ion-Exchange Method for the Synthesis of II–VI Mesoporous Materials

Prior to the discoveries of mesoporous MCM-41[3] and SBA-15,[4] the importance of confining the dimensions of II–VI semiconductor materials in a suitable size-restricting host had been recognized. The microporous nature of zeolites provides an ideal environment for the inclusion of nanosized semiconducting materials. The ionic character of these zeolites offers the opportunity to exchange host cations for desired metal cations in the pursuit of enclosing binary metal chalcogenides within the framework cages. As such the ion-exchange method for the synthesis of II–VI materials in zeolites was developed for the synthesis of CdS in zeolites-X, Y and A.[25] Since that time there have been numerous studies investigating the synthesis of CdS,[26] CdTe[27] and ZnS[28] in various zeolite hosts using this general approach.

The typical procedure uses the sodium form of the respective zeolite. Sodium cations within the framework can be exchanged for preferred metal cations through mechanical mixing of the zeolite with a given metal salt. Generally nitrate salts are used,[25,26a–26c,27,28c] although chloride[26d,26e,28a,28b] and sulfate[28b] salts and even Me_2M (M = Zn, Cd)[28d] have also found utility. The ion-exchanged materials are often calcined at 400 °C and, in the case of the sulfides, are treated with a flow of H_2S at 100 °C. Sulfidization has also been achieved using thiourea[26e] and Na_2S.[28c] An alternative approach has been employed in the formation of CdTe, where tellurium metal is incorporated into the framework of zeolite-A at high temperature prior to cation exchange.[27] A wide variety of zeolites have been investigated in this manner and include zeolite-A,[25b,25c,26c,27] zeolite-X,[25b,25c,26e] zeolite-Y,[25,26d] mordenite[26a,26b,28] and SAPO-5.[26c]

The microporous environment of zeolites used for the encapsulation of semiconducting materials often leads to composite materials which show broad particle size distributions. This generally results from poor channel filling from ion-exchange, ultimately leading to a high density of defect sites. There are reports that clusters, superclusters and aggregates can co-exist within the same host,[26e] and in some instances larger particles are found to passivate the external surface.[28a] Although in most cases quantum-confinement effects are noted by the blue shift in the absorption edge,[26–28] identifying metal chalcogenide material within the host through PXRD is hindered by the overlapping of diffraction peaks of the II–VI material with those of the zeolite framework.[26–28]

Mesoporous materials offer a larger pore diameter for the inclusion of semiconductor materials and may thus offer better control over particle size. The improvement over microporous zeolites is illustrated by a similar ion-exchange method with a commercially available mesoporous zeolite.[29] Using the sodium form of the zeolite, Na^+ is exchanged for Cd^{2+}, and the material is sulfidized with Na_2S at room temperature. Size and loading of CdS can be controlled by varying the amount of Cd^{2+} introduced during the exchange process. From the wide-angle XRD pattern (Figure 6) the observed diffraction peaks are indexed to cubic crystalline zinc blende CdS, where the peaks become sharper as the Cd^{2+} concentration is increased in the material, thus leading to an increase in particle size as determined by the Scherrer formula.[30]

Quantum-confinement effects are readily observed in the photoluminescence (PL) and photoluminescence excitation (PLE) spectra, where two bands are observed in the PL spectra and three bands are present in the PLE spectra. In both, the bands are found to blue shift as particle size de-

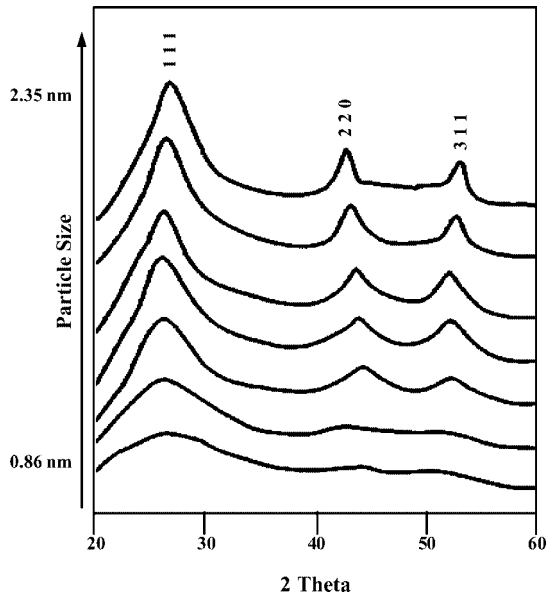

Figure 6. Wide-angle XRD patterns for zinc blende CdS formed in a mesoporous zeolite. Diffraction peaks become sharper as the amount of Cd^{2+} incorporated is increased, thus leading to larger-sized particles. (Figure reprinted and modified from ref.[29], Formation, Structure and Fluorescence of CdS Clusters in a Mesoporous Zeolite, Copyright 1998, with permission from Elsevier).

creases. In the PL spectra the strong Stokes-shifted band at 550 nm arises from trapped luminescence at the surface while a shoulder at 420 nm is assigned to band-edge emission (Figure 7).

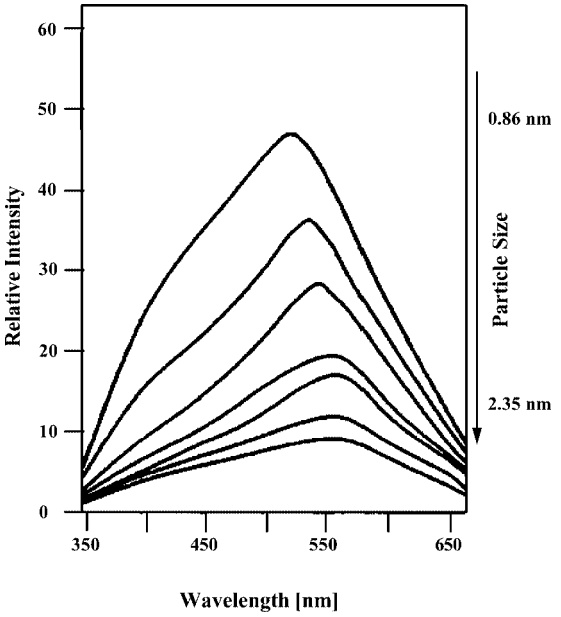

Figure 7. Photoluminescence spectra for zinc blende CdS formed in a mesoporous zeolite. As particle size decreases the emission peaks become blue-shifted. (Figure reprinted and modified from ref.[29], Formation, Structure and Fluorescence of CdS clusters in a Mesoporous Zeolite, Copyright 1998, with permission from Elsevier).

With the advent of MCM-41 and SBA-15 new methods for the incorporation of II–VI materials within a mesoporous framework have been pursued. Typically MCM-41 and SBA-15 are used in their purely siliceous forms, and thus there are no counter-cations that can be exchanged for desired metal ions, hence a modified route to developing metal chalcogenides within the mesopores through ion-loading was designed. Of recent interest has been the synthesis of manganese-doped II–VI semiconductors within a mesoporous host through the use of this method.[31–33] In particular $Zn_{1-x}Mn_xS$,[31] $Cd_{1-x}Mn_xS$[32] and $Cd_{1-x}Mn_xSe$[33] have been synthesized in MCM-41 and SBA-15 to investigate their unique optical and magnetic properties. In this approach metal acetate salts of Zn or Cd are mixed with $Mn(OAc)_2$ and solution loaded into both MCM-41 and SBA-15. Treatment with either H_2S or H_2Se at 100 °C leads to the formation of sulfides and selenides, respectively.

As determined from electron paramagnetic resonance (EPR) spectroscopy, when $x = 0.01$ the resulting encapsulated nanowires are of the zinc blende structure, while in cases where $x > 0.01$ the materials are characteristically found to display the wurtzite structure. This is true in the case of both Zn- and Cd-based materials. The X-ray absorption near-edge structure (XANES) region of the X-ray absorption spectra suggest that Mn^{2+} is present within the composite materials but not in the form of MnS. The results from XANES analyses suggest rather that Mn^{2+} is found to substitute for M^{2+} (M = Zn, Cd) sites within the ME (E = S, Se) structure, thus becoming intimately incorporated within the material. XANES spectra also indicate that only a small percentage of Mn^{2+} is found on the surface of the ME structure. All of the composite materials show quantum-confinement effects that increase with decreasing wire diameter (where the diameter is controlled by the chosen mesoporous host). These quantum-confinement effects ultimately lead to an increase in the direct bandgap energy.

Typically II–VI composite materials prepared using ion-exchange/loading as well as surface functionalization of the mesoporous material (vide infra) are in microcrystalline (powder) form. Although it is important to develop the chemistry using powder-based composites, these powders are generally unfavourable for their application in non-linear optics and optical characterization, where diffuse reflectance techniques are often employed. Thus there has been an emergence in the development of mesoporous thin films,[34–36] monoliths[34] and membranes[37] incorporating II–VI materials. Specifically, CdS[34,35,37] CdSe[35] and CdTe[36] have been prepared in these forms using a similar ion-loading technique, where a cadmium salt is introduced to the mesopores typically during the synthesis of the framework. The general procedure involves the use of alkyl-(ethylene oxide) as the structure-directing agent of which a sol is formed under acidic conditions in the presence of tetraethoxysilane. Cadmium nitrate[34] (or acetate[35]) salts are added to the sol from which thin films are formed by dip-coating, and monoliths are prepared by spreading the sol over a glass slide. Metal chalcogenides are thus formed through exposure to H_2E. An alternative approach used in the synthesis of mesoporous CdTe thin films utilizes the electrochemical codeposition of cadmium sulfate and tel-

lurium dioxide.[36] Prior to electrodeposition, the salts are incorporated into a lytropic liquid crystalline domain composed of octaethyleneglycol monohexadecyl ether as the templating agent. Using a similar synthetic approach as detailed above, porous alumina membranes are used as a template in the formation of CdS mesoporous structures.[37] Using this route, surfactant, silica and cadmium salts are incorporated into the channels of the alumina membrane, followed by H_2S treatment. Much like their powder counterparts, these materials have particle sizes on the order of 2.5 nm when formed in thin films and monoliths and ca. 6 nm when synthesized as a membrane structure. In addition, all enclosed materials display similar quantum-confinement effects to those observed in MCM-41 and SBA-15.

Surface Modification of Mesoporous Hosts for the Synthesis of II–VI Materials

Organic functionalization of the interior pore structure of a mesoporous material has been studied extensively, resulting in the formation of inorganic–organic hybrid materials.[38] Pore modification can be achieved through either a direct co-condensation method[38d–38f] or post-synthesis grafting.[38g–38j] The method of post-synthesis grafting is most often utilized in the inclusion of II–VI semiconductor species within a mesoporous host. This modification procedure exploits the presence of multiple reactive silanol moieties populating the surface of the pore walls. Through condensation reaction with a designated alkoxysilane, the organic functional group is effectively anchored to the pore surface by the formation of silicon–oxygen bonds (Figure 8). Thiol[39] and ethylenediamine[40] moieties can be incorporated into the pore structures of MCM-41 and SBA-15 and have been used as a method of developing and/or confining metal sulfide nanoparticles within the host framework.[41–46] In this vein, these organic groups can meet several objectives which include acting as an anchor for the prepared metal sulfide, enhancing the hydrophobicity of the interior pore structure and, in the case of the anchored thiol moiety, pre-positioning the sulfide source.

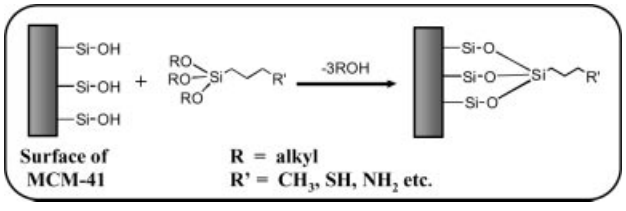

Figure 8. General reaction scheme used in the surface modification of siliceous mesoporous materials, utilizing an alkoxysilane. The rectangular area represents the pore wall of MCM-41 (or SBA-15) populated by surface silanol groups.

Cadmium sulfide is the most comprehensively studied II–VI material that has been encapsulated in a mesoporous host. In particular, the method of organic functionalization has found utility in both the synthesis and constriction of the resulting CdS particles. In studies pertaining to both MCM-41 and SBA-15, the interior pore surface is initially functionalized with 3-(mercaptopropyl)trimethoxysilane in either refluxing or room temperature solvent.[41–43] The degree of functionalization has been shown to be dependant on reaction temperature, where the higher the temperature the greater the extent of modification (as monitored by nitrogen adsorption and IR spectroscopy).[41] Cd^{2+} is adsorbed into the pores through stirring a methanolic solution of $Cd(OAc)_2{\cdot}2H_2O$ with the organo–mesoporous material. The resulting material is treated either with a stream of 5 vol-% H_2S in nitrogen[41,42] or calcined at 300 °C in nitrogen[43] resulting in the formation of CdS nanorods, as depicted in Figure 9.

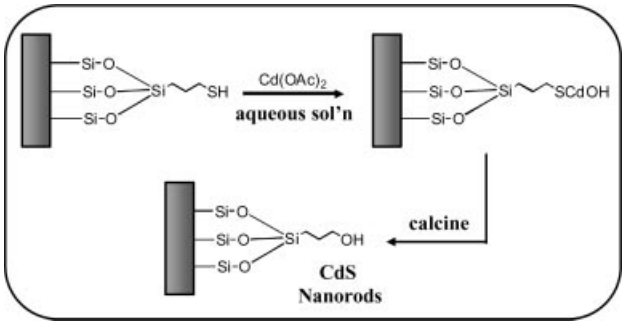

Figure 9. Formation of CdS nanorods in thiol-modified SBA-15 through the addition of $Cd(OAc)_2$ followed by calcination under nitrogen.

The incorporation of CdS nanoparticles within the porous structure is confirmed by wide-angle PXRD and diffuse reflectance UV/Vis spectroscopy. From PXRD analysis, the wide-angle peaks are indexed to the hexagonal cell (wurtzite structure) of CdS, shown in Figure 10, as opposed to the cubic form of CdS generated from the ion-exchange method. The UV/Vis spectra indicate a blue shift in the absorption edge (305–485 nm) of the resulting CdS–mesoporous materials compared to bulk CdS (515 nm), and this blue shift is consistent with the enclosed particles exhibiting quantum-confinement effects. CdS–SBA-15 composite materials are found to show a smaller blue shift of the exciton peak given the larger diameter of the pore, consistent with larger-sized particles confined within the framework.[42] The size, however, of the CdS particles grown in SBA-15 is strictly dependent on the synthetic method employed: H_2S treatment produces smaller-sized particles (3.4 nm),[42] while post-synthesis calcination is found to produce larger-sized particles (6 nm).[43] The sizes for both particles are calculated from the PXRD data using the Scherrer formula.

It has also been demonstrated that the size of the CdS particles grown inside MCM-41 is dependent on both the degree of organic functionalization and the temperature of H_2S treatment.[41] CdS particles grown in MCM-41 with the greatest coverage of thiol moieties are found to grow from 1.2 to 2.2 nm upon changing the temperature of formation from 30 °C to 230 °C. At the highest temperature of formation the particles are found to grow to the available

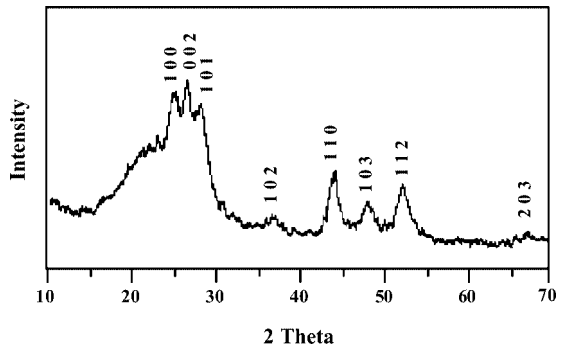

Figure 10. Wide-angle XRD pattern of wurtzite CdS nanorods synthesized within SBA-15. (Figure reprinted and modified from ref.[43], in situ Adsorption Method for Synthesis of Binary Semiconductor CdS Nanocrystals Inside Mesoporous SBA-15, Copyright 2002, with permission from Elsevier).

pore diameter, while at lower temperature there is stronger interaction of Cd^{2+} with the thiol groups, consequently leading to impeded mobility of the metal ions. Conversely, the size of the nanoparticles is found to decrease with increasing surface functionalization, as confirmed by the blue-shifted exciton peak (430 to 320 nm). This result can be correlated with the decreased pore diameter of the functionalized materials with increasing the temperature of modification, thereby reducing the available pore space for nanoparticle growth.

Although the majority of published reports study the incorporation of cadmium chalocogenides in a mesoporous host, there have been fewer cited examples of encapsulated nanosized zinc sulfide. Of these, there are several that utilize organic functionalization of MCM-41 with ethylenediamine as a means of forming ZnS nanoparticles within the framework.[44,45] Surface modification is achieved through refluxing calcined MCM-41 with *N*-[3-(trimethoxysilyl)propyl]ethylenediamine in dry toluene. The anchored chelating group provides the ability to adsorb Zn^{2+} from an ethanolic solution of $Zn(OAc)_2{\cdot}2H_2O$ while stirring at room temperature.

The desired ZnS nanoparticles can then be generated through several approaches. One method involves calcining the resulting Zn–MCM-41 material at 600 °C in air, thus removing all organic constituents from the pore while retaining the adsorbed Zn^{2+}, present in the host as ZnO as a result of calcination.[44] Similar to the formation of CdS materials within MCM-41, both Zn–MCM-41 modified with ethylenediamine and ZnO–MCM-41 are treated with H_2S for up to 6 hours leading to the synthesis of ZnS nanoparticles.[44] Six hours of exposure to H_2S is required to ensure the ratio between Zn and S reaches ca. 1:1, as confirmed by energy dispersion X-ray (EDX) analysis. An alternative method involves mixing the organically modified Zn–MCM-41 with an ethanolic solution of carbon disulfide at room temperature, thus producing ZnS within the pores of MCM-41.[45] In this method, however, no diffraction peaks in the wide-angle XRD are observed for ZnS thus suggesting the incomplete formation of ZnS crystallites at room temperature, however, the ratio of Zn to S is still found to be close to 1:1. This is quite different to the ZnS nanoparticles formed from H_2S treatment,[44] where the diffraction peaks in the wide-angle XRD are indexed to zinc blende ZnS. From this XRD study the ZnS nanoparticles are found to be less than 2.5 nm in size, as determined from the Scherrer formula.

Confirmation that the synthesized particles were located in the interior of the framework vs. the exterior surface was attained from TEM analysis and from thermal treatment of the ZnS–MCM-41 materials.[44] The TEM images show no indication of the formation of ZnS on the exterior pore surface whether the electron beam is parallel or perpendicular to the channel direction. ZnS particles in the pores of MCM-41, however, are not observed directly using TEM, likely due to the weak contrast between ZnS and the silica framework. In the event ZnS particles formed on the external surface of MCM-41, thermal treatment of the composite material should result in the generation of larger-sized particles, given that the exterior pore surface provides no restriction to particle growth. Treating the materials at 150 °C while under vacuum results in no obvious change in the wide-angle XRD, therefore suggesting that all ZnS nanoparticles are confined to the pores of MCM-41 and as such their growth is impeded.

As observed for CdS formed in organically modified mesoporous materials,[41–43] the absorption edge of ZnS confined in MCM-41 (ca. 350 nm) is found to be blue-shifted from that of bulk ZnS (410 nm). Variation in the synthetic method does not result in any appreciable change in the absorption edge whereby the exciton peak of calcined ZnS–MCM-41 is found to be red-shifted by 10–20 nm from that of Zn–MCM-41-containing anchored ethylenediamine. This blue shift from the bulk material is indicative of the resulting materials exhibiting quantum-confinement effects. In both studies[44,45] the photoluminescence properties of the composite materials were investigated. From the PL spectra, the ZnS-MCM-41 materials are found to emit in the blue between 430 and 475 nm, and this has been assigned to defects associated with sulfur vacancies.[44]

Despite the ethylenediamine moiety within the framework, the resulting ZnS nanoparticles are found to leach out of the pores (as observed with TEM analysis) upon stirring for more than 4 hours in aqueous solution, consequently growing into larger-sized particles (Figure 11).[44] This problem is even more pronounced in the case where the ethylenediamine moiety is removed through calcination. To circumvent this problem with leaching, bifunctional mesoporous materials have been designed and offer advantages over monofunctionalized mesoporous materials, especially in the formation of II–VI nanoparticles within the host.[46] This synthesis uses two methods of grafting, where initially ethylenediamine-modified MCM-41 is formed through direct co-condensation[47] followed by post-synthesis grafting of a thiol moiety. The post-synthesis grafting is carried out in supercritical fluid to ensure uniform distribution of the organic groups. CdS nanoparticles are then prepared in the same manner as already described using thioacetamide as the source of S^{2-}. It is believed that the ethyl-

enediamine group strongly chelates Cd^{2+}, while the thiol moiety anchors the formed CdS particles. By releasing Cd^{2+} from ethylenediamine more Cd^{2+} can be adsorbed, ultimately until the pores of MCM-41 are filled entirely with CdS. It is thought that these bifunctional MCM-41 materials can offer a stronger host–guest interaction over conventional monofunctionalized materials[44] while allowing a greater density of binary semiconductor material to fill the pore structure.

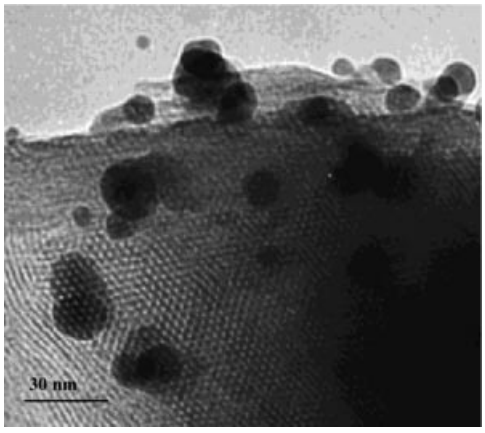

Figure 11. Transmission electron microscope image of ZnS particles leaching out of ethylenediamine-modified MCM-41 after ethanolic treatment. It is apparent from the image that particles aggregate to larger species upon leaching from the channel structure. (Figure reprinted with permission from ref.[44]. Copyright 2001, American Chemical Society).

Surface Functionalization Used to Incorporate Preformed Nanoparticles

In addition to the synthesis of II–VI nanoparticles within a mesoporous host, surface functionalization has also found utility in directing the incorporation of preformed nanoparticles within the modified framework.[48–51] In particular, post-synthesis grafting of an organic thiol is often used to develop a hydrophobic interior to the pore structure, thus promoting the delivery of II–VI nanoparticles into the host. Recent efforts have focused on the synthesis of semiconducting nanoparticles within the hydrophilic core of reverse micelles.[52] The columnar structure of the reverse micelles makes these ideal candidates for their inclusion within MCM-41 and SBA-15. The passivation of the mesoporous surface with a hydrophobic moiety ultimately facilitates the inclusion of the reverse micelles and consequently semiconducting nanoparticles within the siliceous framework.

Cadmium[48–50] and zinc sulfide,[51] formed from reverse micellar solutions, have been encapsulated within MCM-41. The typical procedure uses a reverse micellar solution containing bis(2-ethylhexyl)sulfosuccinate (AOT), water and isooctane. A reverse micellar solution of a specified water content (W_o = [H_2O]/[AOT]) containing either $Cd(NO_3)_2$ or $ZnSO_4$ is added rapidly to a second micellar solution, of equal water content, containing Na_2S. Within minutes the MS (M = Zn, Cd) nanoparticles form and the mesoporous material, modified through post-synthesis grafting of a propyl thiol group, is added to solution. The percent incorporation of MS into the mesoporous host is determined by subtracting the absorbance of MS in the supernatant of the reaction from that of the original reverse micellar solution. The use of large-pore MCM-41 leads to the inclusion of all preformed nanoparticles, as observed by the lack of absorbance for MS in the supernatant.

Nanoparticles of cadmium sulfide are only found to insert into the mesoporous channel if the pore wall has been functionalized with a propyl thiol moiety. The presence of the organic thiol promotes bonding between itself and the encapsulated CdS nanoparticles.[48,49] Although incorporation of CdS is easily achieved in larger-pore systems (ca. 4 nm), the percent incorporation is found to be strongly dependant on the micellar water content (W_o) in medium-pore systems (ca. 3.5 nm) and not at all dependant on W_o in smaller-pore systems (2 nm).[48,49] It is suggested that in large- and medium-pore MCM-41 a particle-sieving effect is observed where percent incorporation decreases with increasing W_o. This can be directly correlated with observed particle size, where smaller-sized particles are formed in micellar solutions with low water content. Consequently, the pore diameter dictates the size of CdS nanoparticles that can enter the framework, where particles exceeding the diameter of the pore will not be encapsulated. Conversely, for smaller-pore MCM-41, all values of W_o lead to more than 90% inclusion of CdS within the framework despite the size of the preformed nanoparticles exceeding the pore diameter. It is believed that these nanoparticles are immobilized in the macropores of MCM-41 (20–40 nm) and on the surface of the framework.

A mechanism for the incorporation of II–VI nanoparticles from reverse micellar solutions into mesoporous frameworks has been proposed.[49] It is believed that water droplets from the reverse micellar solution are absorbed into the pores of the given framework. As such, these droplets contain preformed MS nanoparticles which are transfixed to the pore through anchored thiol groups. Increased loading amounts of MS in the pore structure can be achieved through additional treatment with a second MS micellar solution.[49,51] Exchange of MS-free water droplets for MS-containing water droplets facilitates this process. Although sequential treatment with a MS micellar solution leads to an increased cumulative amount of MS within the framework, the successive increase in MS loading decreases with each treatment.

Diffuse reflectance UV/Vis spectroscopy of the composite MCM-41 materials reveals a blue shift in the absorption onset for CdS (450 nm) and ZnS (272 nm) from the parent bulk materials.[50,51] Although the absorption is very broad, possibly resulting from a distribution of exciton states due to varying particle sizes, these observed blue shifts in absorption onset are consistent with the enclosed particles demonstrating quantum-confinement effects. ZnS particles are found to be ca. 2 nm,[50] while CdS particles are found

to range between 3–3.4 nm[48,50] In all cases, the size of the enclosed particles does not exceed the diameter of the MCM-41 pore.

The PL spectrum (Figure 12) of encapsulated CdS shows two broad emission bands at 430 nm (sub-band I) and 530 nm (sub-band II).[50] The authors attribute the emission at 430 nm to band-edge emission, caused by excitonic recombination, while the largely Stokes-shifted emission at 530 nm is the result of surface-defect states. The emission of sub-band I is blue-shifted (420 nm) upon calcination of the composite material (to remove all organic constituents), as observed in Figure 12b, while the emission of sub-band II is red-shifted (560 nm). These changes in the PL spectrum are associated with the slight reduction of particle size upon calcination. On the other hand, ZnS emits in the spectral region associated with the emission resulting from the modified MCM-41 framework (390 nm), however, the emission due to confined ZnS (373 nm) can be distinguished from that of MCM-41 due to its increased intensity.[51] The emission of ZnS is also found to be enhanced with sequential treatment of ZnS–micellar solutions (Figure 13). Unlike the broad blue emission associated with ZnS formed within modified MCM-41,[44] these enclosed ZnS particles show emission in the UV. Luminescence does thus not result from surface sulfur vacancies but rather from recombination processes at core lattice sulfur vacancies. This is further confirmed by the PLE spectrum that is centred at 308 nm, and hence the observed emission is Stokes-shifted from the corresponding PLE spectrum. Confined CdS is found to have both fast (ca. 0.1 ns) and slow (5–13 ns) lifetime components associated with band-edge and Stokes-shifted emission, respectively, while encapsulated ZnS was found to have a single recombination lifetime of 1.3 ns resulting from a highly selective emission state.[50,51]

Surface modification of the silicate framework is not necessary to encapsulate II–VI nanoparticles prepared in reverse micelles into the mesoporous host if a gas antisolvent technique (supercritical CO_2) is used, rather than solution loading of the reverse micelles.[53] It has been found that by adding compressed CO_2 to a MS–micellar solution leads to the removal of MS nanoparticles from the hydrophilic core of the micelle.[54] ZnS has been loaded into MCM-41 using this technique, where CO_2 is added to a dispersion of ZnS–reverse micelles and calcined MCM-41.[53] Upon removing ZnS from the reverse micelles, the nanoparticles can diffuse into the pores of MCM-41 and are thus absorbed by the pore wall. In the absence of CO_2, ZnS is not found to be enclosed within the pores of MCM-41 and therefore the antisolvent behaviour of CO_2 is necessary for their inclusion.

In addition to modifying the framework with propyl thiol groups, to be used to attach preformed CdS to the mesoporous host, other organic modifiers have been used. Zn-doped SBA-15 has been modified with an alkane dithiol moiety, where Zn–S bond formation anchors the organic to the pore wall.[55] The pendant thiol provides a hydrophobic interior to the pore structure thus allowing the movement of CdS–reverse micelles into the framework. The incorporation of Zn is required to enhance the photocatalytic activity for H_2 generation of the resulting composite materials.

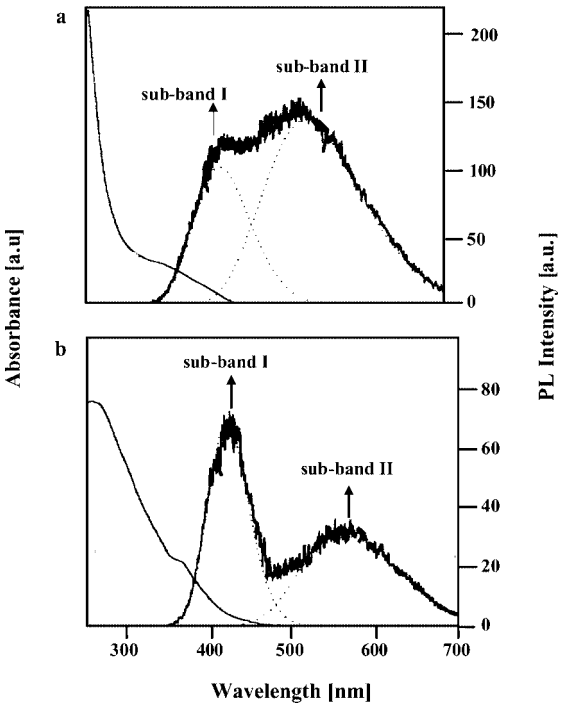

Figure 12. Diffuse reflectance UV/Vis spectra (solid line) and PL spectra of CdS encapsulated into thiol–modified MCM-41: a) as-synthesized composite material and b) after calcination of CdS–MCM-41 material. (Figure reprinted and modified from ref.[50], Emission Characteristics of CdS Nanoparticles Induced by Confinement within MCM-41 Nanotubes, Copyright 2002, with permission from Elsevier).

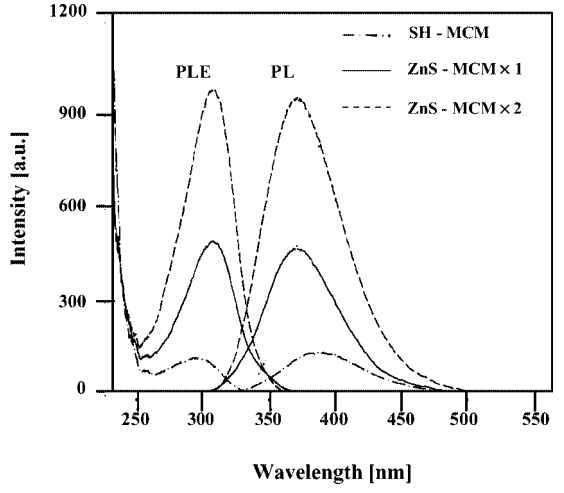

Figure 13. PL and PLE spectra of thiol-modified MCM-41, ZnS–MCM-41 after first exposure to ZnS–reverse micellar solution and ZnS–MCM-41 after two treatments with ZnS–reverse micellar solutions. (Figure adapted with permission from ref.[51]. Copyright 2004, American Chemical Society).

The utility of functionalizing the pore wall to promote nanoparticle attachment has shown promise in the field of stimuli-responsive controlled-release drug-delivery systems.[56] A mesoporous silica nanosphere (having MCM-41

type hexagonally packed mesopores) can be modified with (2-propyldisulfanyl)ethylamine, following which drug molecules such as vancomycin can be absorbed by the material. The openings of the nanosphere are then capped by mercaptoacetic acid-derived CdS through the formation of amide bonds to the organic anchor. The lability of the disulfide bond existing between the nanosphere and CdS allows for facile bond cleavage with various disulfide reducing agents (e.g. mercaptoethanol, dithiothreitol) thereby allowing controlled release of the absorbed drug molecules to the targeted area.

Preformed Clusters Used for the Formation of II–VI Materials in Mesoporous Hosts

Incorporating clusters within mesoporous frameworks has been studied extensively,[57] and the development of condensed nanoparticle structures within the framework from these cluster precursors is also of interest.[57a–57d] Recently, it was demonstrated that $[Cu_6(TePh)_6(PPh_2Et)_5]$ can be loaded into the pores of MCM-41 at 110 °C.[58] As a discrete molecule, the cluster is known to undergo a series of condensation reactions through photochemical elimination of Ph_2Te to yield $[Cu_{50}(TePh)_{20}Te_{17}(PPh_2Et)_8]^{4-}$.[59] This same photochemical behaviour was observed for the Cu_6 cluster enclosed in MCM-41 as marked by the red shift (440 nm) in the UV/Vis absorption spectrum upon irradiation, from that of the original Cu_6 cluster (249 nm). Thermal condensation of the cluster is found to lead to the formation of Cu_2Te nanoparticles within the host.[58b]

The hexagonally arranged channel structure of MCM-41 and SBA-15 makes these materials ideal candidates for the formation of nanowire arrays.[60] The siliceous framework acts as a hard-surface template that can be removed after formation of the desired nanowire assemblies. This template technique has been employed in the formation of CdS nanowires within SBA-15.[61,62] The method initially requires impregnation of a precursor cluster, containing both Cd and S within a single source. The resulting materials are treated thermally to promote cluster decomposition to CdS, upon which the siliceous framework is etched away from the surface of the CdS nanowires through treatment with aqueous NaOH.

In one method, $Cd(NO_3)_2{\cdot}4H_2O$ is combined with thiourea in an ethanolic solution to which a suspension of SBA-15 is added.[61] The mixture of $Cd(NO_3)_2$ with thiourea leads to the formation of complex cadmium–thiourea precursors. Upon evaporating ethanol from the suspended materials, the cadmium–thiourea precursors are incorporated into the channels of SBA-15 by capillary condensation. In heating the materials to 150 °C, (cubic) zinc blende CdS nanowires are formed, as confirmed by wide-angle XRD and high-resolution TEM analysis. Alternatively, cadmium thioglycolate $[Cd_{10}S_{16}C_{32}H_{80}N_4O_{28}]$ has been used as a Cd–S single source precursor in SBA-15, followed by thermal treatment thus leading to the formation of (hexagonal) wurtzite CdS as observed by wide-angle XRD and selected area electron diffraction (SAED).[62] From TEM analysis, the CdS assembly appears as a hexagonal array of nanowires having a diameter of ca. 6 nm and a particle spacing of ca. 3 nm. TEM analysis also indicates that the nanowire array is exactly an inverse replica of SBA-15. EDX confirmed the 1:1 ratio between Cd and S with negligible contribution from Si.

A similar single-source-precursor approach has also been utilized in the formation of CdS within Al–MCM-41 and zeolitic mordenite.[63] Initially $CdCl_2$ and thiourea are added to the silica materials and then treated thermally to promote the formation of CdS. EDX results, however, suggest lower sulfur content than the expected (1:1, Cd:S), which could potentially lead to vacancies and defects within the materials. In these materials the siliceous framework is maintained, and as a result a broad size distribution of nanoparticles is observed. Smaller-sized particles are found to be enclosed within the Al–MCM-41 host, while larger particles are immobilized on the external surface. Conversely, the zeolite is only found to contain CdS on the exterior surface.

In the revision stage of this microreview a new synthetic methodology exploiting a molecular single-source-precursor approach in the formation of cadmium chalcogenides was reported.[64] Using melt permeation, the molecular precursors TMEDA-$Cd(EPh)_2$ (where TMEDA = tetramethylethylenediamine and E = S, Se, Te) are incorporated into the mesopores of SBA-15. Through subsequent pyrolysis of the encapsulated precursors, CdS, CdSe and CdTe nanoparticles are formed within the pores of SBA-15, having a particle size of roughly 7 nm. The given cadmium chalcogenide forms in the most thermodynamically favoured polymorph; CdS as wurtzite, CdTe as zinc blende and CdSe as a mixture of both the wurtzite and zinc blende forms.

Quantum-Dot Doping in Mesoporous Materials

The recent use of quantum dot (QD) and quantum wire (QW) cadmium chalcogenides in device fabrication has led to the development of LEDs, biological probes and field-effect thin-film transistors with tunable properties.[65] One of the major obstacles in fostering new devices of one-, two-, and three-dimensional QD arrays is being able to manipulate and control their spatial orientation. As such, mesoporous hosts offer an ideal environment for controlling the organization of QDs.[66,67]

A recent example has been detailed, where CdSe nanoparticles are synthesized in the pores of MCM-41, combining the methods of solution loading and hot injection into a coordinating medium.[66] There have been many examples on the growth of nanoparticles in a highly coordinating solvent (e.g. trioctylphosphane oxide – TOPO)[18b,68] but none that has extended this technique to the inclusion of such nanoparticles within MCM-41. In this approach, Me_2Cd and Se (dissolved in tributylphosphane) are encapsulated into the pores of MCM-41. The wet suspension is rapidly injected into hot TOPO (325 °C), thereby initiating the

growth of CdSe. Upon completion the materials are washed repeatedly with toluene to remove excess TOPO and larger CdSe nanoparticles that may have grown on the exterior surface. UV/Vis spectroscopy of the resulting composite material indicates a blue shift in absorption maxima from that of bulk CdSe suggesting the encapsulated nanoparticles exhibit characteristic quantum-confinement effects. X-ray photoelectron spectroscopy (XPS) of Cd and Se show broad asymmetric peaks indicating there could possibly be multiple bonding domains. Either Cd or Se could react with surface silanols of MCM-41, hence Si–O–Cd or Si–O–Se bonding interactions have been proposed.

Preformed core–shell QDs of ZnS-capped CdSe have been loaded into the pores of mesoporous beads whose surface is covered with hydrocarbons.[67] The QDs are confined into the pores through interdigitation of the hydrocarbon and surface TOPO on the nanoparticle. These materials were found to exhibit higher luminescence than latex and nonporous polystyrene beads doped with similar QDs.

Preventing Particle Aggregation with Exterior Surface Functionalization

One limitation to the approaches used to incorporate II–VI materials within a mesoporous host is the potential to form large aggregated nanoparticles on the exterior surface. Recent efforts have focused on the selective functionalization of mesoporous materials, where exterior functionalization can be performed prior to removal of the structure-directing agent (surfactant).[69] Upon removing the surfactant, internal grafting can be achieved in a similar manner as has been described earlier (vide supra).

The success of external grafting has led to its use in the inclusion of II–VI materials within MCM-41 and SBA-15.[70–73] External grafting has demonstrated utility in both the ion-exchange approach[70,71] as well as in the internal pore functionalization method.[72,73]

Cadmium sulfide has been synthesized in a mesoporous host using an ion-exchange approach that incorporates exterior surface modification with phenyltrimethoxysilane.[70,71] Removal of the protonated surfactant renders cationic vacancies within the framework that can be filled by Cd^{2+} in the form of $Cd(OAc)_2$. Similar to the conventional ion-exchange method, this Cd^{2+}–mesoporous material is subsequently sulfidized with H_2S forming CdS exclusively within the pores of both MCM-41[70] and SBA-15.[71] The motivation of this method is that the surface phenyl groups create a hydrophobic coverage of the outer pore surface, and thus the pore interior is the only environment to which Cd^{2+} absorbs. The UV/Vis spectra for CdS, formed in both MCM-41 and SBA-15, show a blue shift in the absorption onset (450 nm and 470 nm, respectively) suggesting that the confined materials exhibit quantum-confinement effects. In addition, the wide-angle XRD of both composite materials indicate the formation of cubic crystalline CdS having a size of < 2.5 nm and 3 nm in MCM-41 and SBA-15, respectively, as determined by the Scherrer formula.

External passivation of SBA-15 with chlorotrimethylsilane, followed by internal functionalization with (3-aminopropyl)triethoxysilane (Figure 14) has led to the successful incorporation of quantum-confined CdSe[72] and CdS.[73] In the case of CdSe, $Cd(NO_3)_2$ is solution-loaded into amino-functionalized SBA-15 that has previously undergone surface functionalization, thus promoting the complexation of Cd^{2+} with the NH_2 groups. After incorporation of Cd^{2+}, the composite material is exposed to sodium selenosulfate (Na_2SeSO_3) under basic conditions (pH, 8). In the presence of a basic medium, Cd^{2+} is converted to $Cd(OH)_2$, while $SeSO_3^{2-}$ gradually releases Se^{2-} within the pores. Se^{2-} readily replaces the hydroxy groups bound to Cd^{2+} due to the lower solubility of CdSe vs. $Cd(OH)_2$. Alkaline conditions are required to promote the formation of CdSe, as similar attempts using a pH < 8 resulted in no reaction.

In a slightly modified procedure, CdS[73] was incorporated into SBA-15 with exterior modification and interior amino functionalization. In this example the chalcogen is added to the framework prior to the metal: Mercaptoacetic

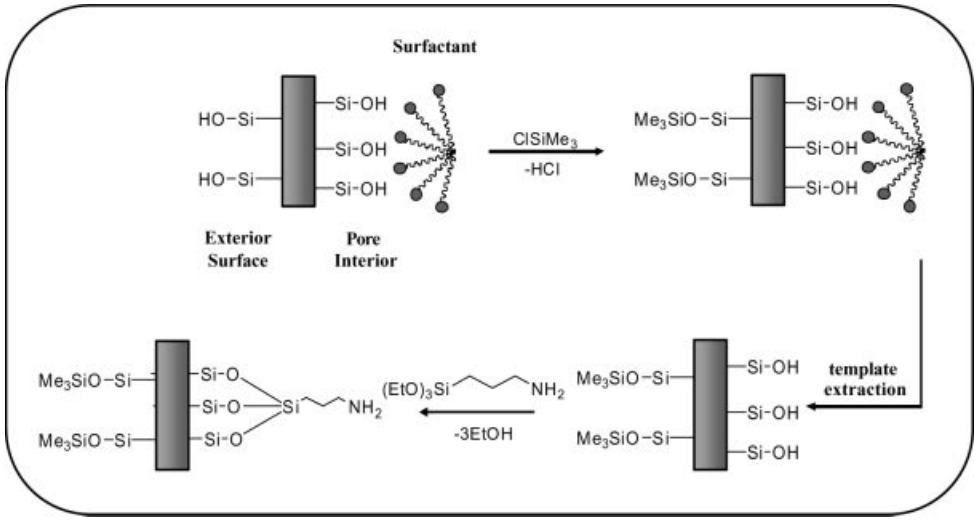

Figure 14. Synthetic pathway used for exterior functionalization followed by interior pore modification with a second organic molecule.

acid in KOH is added to surfactant-free SBA-15. The FTIR spectrum of thiol-SBA-15 indicates the appearance of two stretching vibrations associated with $–COO^–$ that are slightly blue-shifted (1380 and 694 $cm^{–1}$) accompanied by an additional red-shifted peak (1630 $cm^{–1}$) related to $–NH_3^+$ distortion. The shift in these three IR peaks suggests binding of $COO^–$ and NH_3^+. The authors report that mercaptoacetic acid ionizes H^+, which combines with amine to form $–NH_3^+$. This observed coordination between $–COO^–$ and $–NH_3^+$ is what effectively anchors the sulfur source to the framework. Solution loading of $Cd(NO_3)_2$ followed by calcination at 300 °C leads to the formation of CdS.

The UV/Vis spectra for both CdS (519 nm) and CdSe–SBA-15 (622 nm) materials thus prepared show a blue shift in the absorption onset from that of the parent bulk materials; 550 nm and 698 nm, respectively. If no surface modification is employed in the case of CdSe, the absorption onset is only slightly shifted (660 nm) from that of the bulk material, indicating the formation of larger particles. Thus, the overall effect of exterior functionalization leads to smaller particles (5 and 7 nm for CdS and CdSe, respectively) that are found solely within the pores of the host framework.

Conclusions

Mesoporous environments, such as MCM-41 and SBA-15, have been readily used in the quantum confinement of II–VI materials. The unique nanosized siliceous channels are ideal for the inclusion of nanoparticle species. As such, there are several routes that can be employed in the synthesis of II–VI composites, in particular those accessing CdS, CdSe and ZnS particles. The ionic nature of these mesoporous hosts enables ion-exchange of framework ions for desired metal cations that can be successively used to form sulfide and selenide binary materials within the channel structure. An alternative route exploits the multiple silanol moieties populating the interior pore surface, whereby the choice of an appropriate alkoxysilane leads to the formation of new Si–O–Si bonding interactions, thus effectively anchoring an organic functional group to the pore walls. Anchored organic moieties have shown to be valuable in synthesizing, securing and directing II–VI nanoparticles into the interior pore structure. Perhaps a limitation of both these methods is the potential to form aggregated species on the exterior pore surface. In an effort to circumvent this issue and possibly access monodisperse or nearly monodisperse particles within the framework, exterior surface modification has been combined with the methods of ion-exchange and interior pore functionalization. Thus the exterior surface is protected by a hydrophobic layer thereby preventing M^{2+} from adsorbing to the exterior pore walls.

All of the described synthetic routes lead to quantum-confined materials which can be monitored by the blue shifts in the absorption onset from that of the bulk II–VI material. In addition, depending on the synthetic method employed, different polymorphs of the same binary material can be obtained. Although the above methods have been met with a significant amount of success, there is still a tremendous need to develop and explore this field fully. In particular, future studies should be geared towards rationally developing nanoparticle vs. nanowire assemblies within the mesoporous host. As such, researchers need to devise specific synthetic routes that will ultimately generate either nanowire or nanoparticle materials.

The developments presented in this microreview have pioneered the field of quantum-confined materials within mesoporous hosts. With the rapidly and vastly growing interest in nanoparticle construction, the next few years will see an evolution in the area of mesoporous encapsulated II–VI materials.

[1] a) F.-S. Xiao, S. Qiu, W. Pang, R. Xu, *Adv. Mater.* **1999**, *11*, 1091–1099; b) A. Corma, *Chem. Rev.* **1997**, *97*, 2373–2419; c) U. Ciesla, F. Schüth, *Microporous Mesoporous Mater.* **1999**, *27*, 131–149; d) R. C. Schroden, A. Stein, *Colloids and Colloid Assemblies* (Ed.: F. Caruso), Wiley-VCH, Weinheim (Germany), **2004**, 465–493.

[2] K. S. W. Sing, D. H. Everett, R. A. W. Haul, L. Moscou, R. A. Pierotti, J. Rouquérol, T. Siemieniewska, *Pure Appl. Chem.* **1985**, *57*, 603–619.

[3] a) C. T. Kresge, M. E. Leonowicz, W. J. Roth, J. C. Vartuli, J. S. Beck, *Nature* **1992**, *359*, 710–712; b) J. S. Beck, J. C. Vartuli, W. J. Roth, M. E. Leonowicz, C. T. Kresge, K. D. Schmitt, C. T.-W. Chu, D. H. Olson, E. W. Sheppard, S. B. McCullen, J. B. Higgins, J. L. Schlenker, *J. Am. Chem. Soc.* **1992**, *114*, 10834–10843.

[4] a) D. Zhao, J. Feng, Q. Huo, N. Melosh, G. H. Fredrickson, B. F. Chmelka, G. D. Stucky, *Science* **1998**, *279*, 548–552; b) D. Zhao, Q. Huo, J. Feng, B. F. Chmelka, G. D. Stucky, *J. Am. Chem. Soc.* **1998**, *120*, 6024–6036.

[5] a) C.-Y. Chen, S. L. Burkett, H.-X. Li, M. E. Davis, *Microporous Mater.* **1993**, *2*, 27–34; b) J. C. Vartuli, C. T. Kresge, M. E. Leonowicz, A. S. Chu, S. B. McCullen, I. D. Johnson, E. W. Sheppard, *Chem. Mater.* **1994**, *6*, 2070–2077; c) C.-F. Cheng, Z. Luan, J. Klinowski, *Langmuir* **1995**, *11*, 2815–2819.

[6] a) C.-Y. Chen, J.-X. Li, M. E. Davis, *Microporous Mater.* **1993**, *2*, 17–26; b) J. S. Beck, J. C. Vartuli, *Curr. Opin. Solid State Mater. Sci.* **1996**, *1*, 76–87; c) V. Y. Gusev, X. Feng, Z. Bu, G. L. Haller, J. A. O'Brien, *J. Phys. Chem.* **1996**, *100*, 1985–1988; d) M. Kruk, M. Jaroniec, A. Sayari, *J. Phys. Chem. B* **1997**, *101*, 583–589; e) M. Kruk, M. Jaroniec, A. Sayari, *Chem. Mater.* **1999**, *11*, 492–500; f) M. Kruk, M. Jaroniec, C. H. Ko, R. Ryoo, *Chem. Mater.* **2000**, *12*, 1961–1968; K. Morishige, M. Ito, *J. Chem. Phys.* **2002**, *117*, 8036–8041.

[7] K. Moller, T. Bein, *Chem. Mater.* **1998**, *10*, 2950–2963.

[8] a) A. Sayari, *Chem. Mater.* **1996**, *8*, 1840–1852; b) A. Corma, *Top. Catal.* **1997**, *4*, 249–260; c) F. Schüth, A. Wingen, J. Sauer, *Microporous Mesoporous Mater.* **2001**, *44–45*, 465–476.

[9] a) J. M. Kisler, A. Dähler, G. W. Stevens, A. J. O'Connor, *Microporous Mesoporous Mater.* **2001**, *44–45*, 769–774; b) Y. Shiraishi, G. Nishimura, T. Hirai, I. Komasawa, *Ind. Eng. Chem. Res.* **2002**, *41*, 5065–5070; c) B. L. Newalkar, N. V. Choudary, P. Kumar, S. Komarneni, T. S. G. Bhat, *Chem. Mater.* **2002**, *14*, 304–309.

[10] a) K. Tajima, T. Aida, *Chem. Commun.* **2000**, 2399–2412; b) A. M. Showkat, K.-P. Lee, A. I. Gopalan, M.-S. Kim, S.-H. Choi, H.-D. Kang, *Polymer* **2005**, *46*, 1804–1812; c) M. Choi, F. Kleitz, D. Liu, H. Y. Lee, W.-S. Ahn, R. Ryoo, *J. Am. Chem. Soc.* **2005**, *127*, 1924–1932.

[11] R. Mokaya, *J. Phys. Chem. B* **1999**, *103*, 10204–10208.

[12] a) N. Coustel, F. Di Renzo, F. Fajula, *J. Chem. Soc., Chem. Commun.* **1994**, 967–968; b) C.-F. Cheng, W. Zhou, J. Klinowski, *Chem. Phys. Lett.* **1996**, *263*, 247–252.

[13] A. Sayari, P. Liu, M. Kruk, M. Jaroniec, *Chem. Mater.* **1997**, *9*, 2499–2506.

[14] H. Lao, C. Detellier, *Comprehensive Supramolecular Chemistry* (Eds.: J. E. D. Davies, J. A. Ripmeester), Pergamon, **1996,** vol. 8, 277–306.

[15] S. Brunauer, P. H. Emmett, E. Teller, *J. Am. Chem. Soc.* **1938**, *60*, 309–319.

[16] E. P. Barrett, L. G. Joyner, P. P. Halenda, *J. Am. Chem. Soc.* **1951**, *73*, 373–380.

[17] a) C. Lastoskie, K. E. Gubbins, N. Quirke, *J. Phys. Chem.* **1993**, *97*, 4786–4796; b) P. I. Ravikovitch, S. C. Ó Domhnaill, A. V. Neimark, F. Schüth, K. K. Unger, *Langmuir* **1995**, *11*, 4765–4772.

[18] a) L. E. Brus, *J. Chem. Phys.* **1984**, *80*, 4403–4409; b) C. B. Murray, D. J. Norris, M. G. Bawendi, *J. Am. Chem. Soc.* **1993**, *115*, 8706–8715; c) A. P. Alivisatos, *J. Phys. Chem.* **1996**, *100*, 13226–13239; d) L. Brus, *J. Phys. Chem. Solids* **1998**, *59*, 459–465; e) M. Nirmal, L. Brus, *Acc. Chem. Res.* **1999**, *32*, 407–414; f) T. Trindade, P. O'Brien, N. L. Pickett, *Chem. Mater.* **2001**, *13*, 3843–3858; g) N. L. Pickett, P. O'Brien, *Chem. Rec.* **2001**, *1*, 467–479; h) S. Sapra, D. D. Sarma, *The Chemistry of Nanomaterials Synthesis, Properties and Applications* (Eds.: C. N. R. Rao, A. Müller, A. K. Cheetham), Wiley-VCH, Weinheim (Germany), **2004**, vol 2, 371–404.

[19] J. H. Adair, T. Li, T. Kido, K. Havey, J. Moon, J. Mecholsky, A. Morrone, D. R. Talham, M. H. Ludwig, L. Wang, *Mater. Sci. Eng. R. Rep.* **1998**, *23*, 139–242.

[20] a) R. Premachandran, S. Banerjee, V. T. John, G. L. McPherson, J. A. Akkara, D. L. Kaplan, *Chem. Mater.* **1997**, *9*, 1342–1347; b) S. H. Liu, X. F. Qian, J. Yin, X. D. Ma, J. Y. Yuan, Z. K. Zhu, *J. Phys. Chem. Solids* **2003**, *64*, 455–458.

[21] a) A. A. Guzelian, U. Banin, A. V. Kadavanich, X. Peng, A. P. Alivisatos, *Appl. Phys. Lett.* **1996**, *69*, 1432–1434; b) M. Green, P. O'Brien, *Chem. Commun.* **1999**, 2235–2241; c) M. Green, P. O'Brien, *Chem. Commun.* **2000**, 183–184.

[22] a) H. S. Zhou, H. Sasahara, I. Honma, H. Komiyama, J. W. Haus, *Chem. Mater.* **1994**, *6*, 1534–1541; b) M. A. Malik, P. O'Brien, N. Revaprasadu, *Chem. Mater.* **2002**, *14*, 2004–2010; c) T. Mokari, U. Banin, *Chem. Mater.* **2003**, *15*, 3955–3960.

[23] C. E. Housecroft, A. G. Sharpe, *Inorganic Chemistry*, Pearson Education Limited, **2001**, 129–132.

[24] F. A. Cotton, G. Wilkinson, *Advanced Inorganic Chemistry A Comprehensive Text* 3rd ed., Interscience Publishers, **1972**, 511.

[25] a) Y. Wang, N. Herron, *J. Phys. Chem.* **1987**, *91*, 257–260; b) Y. Wang, N. Herron, *J. Phys. Chem.* **1988**, *92*, 4988–4994; c) N. Herron, Y. Wang, M. M. Eddy, G. D. Stucky, D. E. Cox, K. Moller, T. Bein, *J. Am. Chem. Soc.* **1989**, *111*, 530–540.

[26] a) H. Villavicencio-García, M. Hernández-Vélez, O. Sánchez-Garrido, J. M. Martínez-Duart, J. Jiménez, *Solid-State Electron.* **1999**, *43*, 1171–1175; b) R. J. Martín-Palma, M. Hernández-Vélez, I. Díaz, H. Villavicencio-García, M. M. García-Poza, J. M. Martínez-Duart, J. Pérez-Pariente, *Mater. Sci. Eng. C* **2001**, *15*, 163–166; c) A. Aparisi, V. Fornés, F. Márquez, R. Moreno, C. López, F. Meseguer, *Solid-State Electron.* **1996**, *40*, 641–645; d) H. Yahiro, T. Kyakuno, G. Okada, *Top. Catal.* **2002**, *19*, 193–195; e) M. Sotelo-Lerma, M. A. Quevedo-López, R. A. Orozco-Terán, R. Ramírez-Bon, F. J. Espinoza-Beltrán, *J. Phys. Chem. Solids* **1998**, *59*, 145–149.

[27] E. S. Brigham, C. S. Weisbecker, W. E. Rudzinski, T. E. Mallouk, *Chem. Mater.* **1996**, *8*, 2121–2127.

[28] a) M. M. García, H. Villavicencio, M. Hernández-Vélez, O. Sánchez, J. M. Martínez-Duart, *Mater. Sci. Eng. C* **2001**, *15*, 101–104; b) O. Raymond, H. Villavicencio, V. Petranovskii, J. M. Siqueiros, *Mater. Sci. Eng. A* **2003**, *360*, 202–206; c) F. Iacomi, *Surf. Sci.* **2003**, *532–535*, 816–821; d) G. A. Ozin, M. R. Steele, A. J. Holmes, *Chem. Mater.* **1994**, *6*, 999–1010.

[29] W. Chen, Y. Xu, Z. Lin, Z. Wang, L. Lin, *Solid State Commun.* **1998**, *105*, 129–134.

[30] a) P. Scherrer, *Nachr. Ges. Wiss. Göttingen* **1918**, 96–100; b) A. L. Patterson, *Phys. Rev.* **1939**, *54*, 978–982.

[31] a) L. Chen, P. J. Klar, W. Heimbrodt, F. J. Brieler, M. Fröba, H.-A. Krug von Nidda, T. Kurz, A. Loidl, *J. Appl. Phys.* **2003**, *93*, 1326–1328; b) L. Chen, P. J. Klar, W. Heimbrodt, F. J. Brieler, M. Fröba, *J. Supercond.* **2003**, *16*, 99–102; c) F. J. Brieler, P. Grundmann, M. Fröba, L. Chen, P. J. Klar, W. Heimbrodt, H.-A. Krug von Nidda, T. Kurz, A. Loidl, *J. Am. Chem. Soc.* **2004**, *126*, 797–807.

[32] a) L. Chen, P. J. Klar, W. Heimbrodt, F. Brieler, M. Fröba, *Appl. Phys. Lett.* **2000**, *76*, 3531–3533; b) L. Chen, P. J. Klar, W. Heimbrodt, F. Brieler, M. Fröba, H.-A. Krug von Nidda, A. Loidl, *Physica E* **2001**, *10*, 368–372; c) F. J. Brieler, M. Fröba, L. Chen, P. J. Klar, W. Heimbrodt, H.-A. Krug von Nidda, A. Loidl, *Chem. Eur. J.* **2002**, *8*, 185–194; d) F. J. Brieler, P. Grundmann, M. Fröba, L. Chen, P. J. Klar, W. Heimbrodt, H.-A. Krug von Nidda, T. Kurz, A. Loidl, *Chem. Mater.* **2005**, *17*, 795–803.

[33] L. Chen, H. Falk, P. J. Klar, W. Heimbrodt, F. Brieler, M. Fröba, H.-A. Krug von Nidda, A. Loidl, Z. Chen, Y. Oka, *Phys. Status Solidi B* **2002**, *229*, 31–34.

[34] C. Tura, N. Coombs, Ö. Dag, *Chem. Mater.* **2005**, *17*, 573–579.

[35] M. Wark, H. Wellmann, J. Rathousky, *Thin Solid Films* **2004**, *458*, 20–25.

[36] I. S. Nandhakumar, T. Gabriel, X. Li, G. S. Attard, M. Markham, D. C. Smith, J. J. Baumberg, *Chem. Commun.* **2004**, 1374–1375.

[37] W.-S. Chae, S.-W. Lee, S.-J. Im, S.-W. Moon, W.-C. Zin, J.-K. Lee, Y.-R. Kim, *Chem. Commun.* **2004**, 2554–2555.

[38] a) A. Stein, B. J. Melde, R. C. Schroden, *Adv. Mater.* **2000**, *12*, 1403–1419; b) A. Sayari, S. Hamoudi, *Chem. Mater.* **2001**, *13*, 3151–3168; c) M. H. Lim, A. Stein, *Chem. Mater.* **1999**, *11*, 3285–3295; d) T. Asefa, M. J. MacLachlan, N. Coombs, G. A. Ozin, *Nature* **1999**, *402*, 867–871; e) N. Igarashi, K. Hashimoto, T. Tatsumi, *J. Mater. Chem.* **2002**, *12*, 3631–3636; f) M. Jia, A. Seifert, M. Berger, H. Giegengack, S. Schulze, W. R. Thiel, *Chem. Mater.* **2004**, *16*, 877–882; g) A. Cauvel, G. Renard, D. Brunel, *J. Org. Chem.* **1997**, *62*, 749–751; h) B. M. Choudary, M. Lakshmi Kantam, P. Sreekanth, T. Bandopadhyay, F. Figueras, A. Tuel, *J. Mol. Catal. A: Chem.* **1999**, *142*, 361–365; i) C. D. Nunes, A. A. Valente, M. Pillinger, A. C. Fernandes, C. C. Romão, J. Rocha, I. S. Gonçalves, *J. Mater. Chem.* **2002**, *12*, 1735–1742; j) M. Alvaro, A. Corma, D. Das, V. Fornés, H. García, *J. Catal.* **2005**, *231*, 48–55.

[39] a) X. Feng, G. E. Fryxell, L.-Q. Wang, A. Y. Kim, J. Liu, K. M. Kemner, *Science* **1997**, *276*, 923 –926; b) L. Mercier, T. J. Pinnavaia, *Adv. Mater.* **1997**, *9*, 500–503; c) A. M. Liu, K. Hidajat, S. Kawi, D. Y. Zhao, *Chem. Commun.* **2000**, 1145–1146; d) M. H. Lim, C. F. Blanford, A. Stein, *Chem. Mater.* **1998**, *10*, 467–470.

[40] a) J. F. Díaz, K. J. Balkus, F. Bedioui, V. Kurshev, L. Kevan, *Chem. Mater.* **1997**, *9*, 61–67; b) W.-H. Zhang, J.-L. Shi, L.-Z. Wang, D.-S. Yan, *Chem. Mater.* **2000**, *12*, 1408–1413; c) Y. S. Cho, J. C. Park, B. Lee, Y. Kim, J. Yi, *Catal. Lett.* **2002**, *81*, 89–96.

[41] H. Wellmann, J. Rathousky, M. Wark, A. Zukal, G. Schulz-Ekloff, *Microporous Mesoporous Mater.* **2001**, *44–45*, 419–425.

[42] W. Xu, Y. Liao, D. L. Akins, *J. Phys. Chem. B* **2002**, *106*, 11127–11131.

[43] F. Gao, Q. Lu, D. Zhao, *Chem. Phys. Lett.* **2002**, *360*, 585–591.

[44] W.-H. Zhang, J.-L. Shi, H.-R. Chen, Z.-L. Hua, D.-S. Yan, *Chem. Mater.* **2001**, *13*, 648–654.

[45] H. Xi, X. Qian, J. Yin, L. Bian, R. He, Z. Zhu, *Mater. Lett.* **2003**, *57*, 2657–2661.

[46] W.-H. Zhang, X.-B. Lu, J.-H. Xiu, Z.-L. Hua, L.-X. Zhang, M. Robertson, J.-L. Shi, D.-S. Yan, J. D. Holmes, *Adv. Funct. Mater.* **2004**, *14*, 544–552.

[47] a) M. A. Markowitz, J. Klaehn, R. A. Hendel, S. B. Qadriq, S. L. Golledge, D. G. Castner, B. P. Gaber, *J. Phys. Chem. B.* **2000**, *104*, 10820–10826; b) T. Yokoi, H. Yoshitake, T. Tatsumi, *J. Mater. Chem.* **2004**, *14*, 951–957.

[48] T. Hirai, H. Okubo, I. Komasawa, *J. Phys. Chem. B* **1999**, *103*, 4228–4230.
[49] T. Hirai, H. Okubo, I. Komasawa, *J. Colloid Interface Sci.* **2001**, *235*, 358–364.
[50] W.-S. Chae, J.-H. Ko, I.-W. Hwang, Y.-R. Kim, *Chem. Phys. Lett.* **2002**, *365*, 49–56.
[51] W.-S. Chae, J.-H. Yoon, H. Yu, D.-J. Jang, Y.-R. Kim, *J. Phys. Chem. B* **2004**, *108*, 11509–11513.
[52] a) P. Lianos, J. K. Thomas, *Chem. Phys. Lett.* **1986**, *125*, 299–302; b) C. Petit, M. P. Pileni, *J. Phys. Chem.* **1988**, *92*, 2282–2286; c) M. P. Pileni, L. Motte, C. Petit, *Chem. Mater.* **1992**, *4*, 338–345; d) P. Calandra, M. Goffredi, V. Turco Liveri, *Colloids Surf., A* **1999**, *160*, 9–13; e) F. T. Quinlan, J. Kuther, W. Tremel, W. Knoll, S. Risbud, P. Stroeve, *Langmuir* **2000**, *16*, 4049–4051.
[53] J. Zhang, B. Han, Z. Hou, Z. Liu, J. He, T. Jiang, *Langmuir* **2003**, *19*, 7616–7620.
[54] J. Zhang, M. Xiao, Z. Liu, B. Han, T. Jiang, J. He, G. Yang, *J. Colloid Interface Sci.* **2004**, *273*, 160–164.
[55] T. Hirai, M. Nanba, I. Komasawa, *J. Colloid Interface Sci.* **2003**, *268*, 394–399.
[56] C.-Y. Lai, B. G. Trewyn, D. M. Jeftinija, K. Jeftinija, S. Xu, S. Jeftinija, V. S.-Y. Lin, *J. Am. Chem. Soc.* **2003**, *125*, 4451–4459.
[57] a) W. Zhou, J. M. Thomas, D. S. Shephard, B. F. G. Johnson, D. Ozkaya, T. Maschmeyer, R. G. Bell, Q. Ge, *Science* **1998**, *280*, 705–708; b) F. Schweyer, P. Braunstein, C. Estournès, J. Guille, H. Kessler, J.-L. Paillaud, J. Rosé, *Chem. Commun.* **2000**, 1271–1272; c) B. Folch, J. Larionova, Y. Guari, C. Guérin, A. Mehdi, C. Reyé, *J. Mater. Chem.* **2004**, *14*, 2703–2711; d) S. Behrens, G. Spittel, *Dalton Trans.* **2005**, 868–873; e) M. D. Jones, M. J. Duer, S. Hermans, Y. Z. Khimyak, B. F. G. Johnson, J. M. Thomas, *Angew. Chem. Int. Ed.* **2002**, *41*, 4726–4729; f) S. Hermans, S. Sadasivan, C. M. G. Judkins, B. F. G. Johnson, S. Mann, D. Khushalani, *Adv. Mater.* **2003**, *15*, 1853–1857; g) M. D. Jones, M. J. Duer, *Inorg. Chim. Acta* **2003**, *354*, 75–78; h) M. Clemente-León, E. Coronado, A. Forment-Aliaga, P. Amorós, J. Ramírez-Castellanos, J. M. González-Calbet, *J. Mater. Chem.* **2003**, *13*, 3089–3095.
[58] a) C. Kowalchuk, J. F. Corrigan, Y. Huang, *Chem. Commun.* **2000**, 1811–1812; b) C. M. Kowalchuk, G. Schmid, W. Meyer-Zaika, Y. Huang, J. F. Corrigan, *Inorg. Chem.* **2004**, *43*, 173–180.
[59] J. F. Corrigan, D. Fenske, *Angew. Chem. Int. Ed. Engl.* **1997**, *36*, 1981–1983.
[60] a) C.-M. Yang, H.-S. Sheu, K.-J. Chao, *Adv. Funct. Mater.* **2002**, *12*, 143–148; b) P. V. Adhyapak, P. Karandikar, K. Vijayamohanan, A. A. Athawale, A. J. Chandwadkar, *Mater. Lett.* **2004**, *58*, 1168–1171; c) A. A. Eliseev, K. S. Napolskii, A. V. Lukashin, Y. D. Tretyakov, *J. Magn. Magn. Mater.* **2004**, *272–276*, 1609–1611.
[61] X. Liu, B. Tian, C. Yu, B. Tu, Z. Liu, O. Terasaki, D. Zhao, *Chem. Lett.* **2003**, *32*, 824–825.
[62] F. Gao, Q. Lu, D. Zhao, *Adv. Mater.* **2003**, *15*, 739–742.
[63] I. Díaz, M. Hernández-Vélez, R. J. Martín Palma, H. Villavicencio García, J. Pérez Pariente, J. M. Martínez-Duart, *Appl. Phys. A: Mater.* **2004**, *79*, 565–572.
[64] M. Yosef, A. K. Schaper, M. Fröba, S. Schlecht, *Inorg. Chem.* **2005**, *44*, 5890–5896.
[65] a) V. L. Colvin, M. C. Schlamp, A. P. Alivisatos, *Nature* **1994**, *370*, 354–357; b) D. E. Fogg, L. H. Radzilowski, B. O. Dabbousi, R. R. Schrock, E. L. Thomas, M. G. Bawendi, *Macromolecules* **1997**, *30*, 8433–8439; c) B. A. Ridley, B. Nivi, J. M. Jacobson, *Science* **1999**, *286*, 746–749; d) X. Duan, C. Niu, V. Sahi, J. Chen, J. W. Parce, S. Empedocles, J. L. Goldman, *Nature* **2003**, *425*, 274–278; e) J. A. Kloepfer, S. E. Bradforth, J. L. Nadeau, *J. Phys. Chem. B* **2005**, *109*, 9996–10003.
[66] H. Parala, H. Winkler, M. Kolbe, A. Wohlfart, R. A. Fischer, R. Schmechel, H. von Seggern, *Adv. Mater.* **2000**, *12*, 1050–1055.
[67] X. Gao, S. Nie, *J. Phys. Chem. B* **2003**, *107*, 11575–11578.
[68] a) T. Trindade, P. O'Brien, X.-M. Zhang, *Chem. Mater.* **1997**, *9*, 523–530; b) N. Revaprasadu, M. A. Malik, P. O'Brien, M. M. Zulu, G. Wakefield, *J. Mater. Chem.* **1998**, *8*, 1885–1888; c) N. Revaprasadu, M. A. Malik, P. O'Brien, G. Wakefield, *Chem. Commun.* **1999**, 1573–1574; d) P. S. Nair, T. Radhakrishnan, N. Revaprasadu, G. A. Kolawole, P. O'Brien, *Chem. Commun.* **2002**, 564–565.
[69] a) D. S. Shephard, W. Zhou, T. Maschmeyer, J. M. Matters, C. L. Roper, S. Parsons, B. F. G. Johnson, M. J. Duer, *Angew. Chem. Int. Ed.* **1998**, *37*, 2719–2723; b) V. Antochshuk, M. Jaroniec, *Chem. Commun.* **1999**, 2373–2374; c) F. de Juan, E. Ruiz-Hitzky, *Adv. Mater.* **2000**, *12*, 430–432.
[70] Z. Zhang, S. Dai, X. Fan, D. A. Blom, S. J. Pennycook, Y. Wei, *J. Phys. Chem. B* **2001**, *105*, 6755–6758.
[71] S. Wang, D.-G. Choi, S.-M. Yang, *Adv. Mater.* **2002**, *14*, 1311–1314.
[72] Y. Shan, L. Gao, S. Zheng, *Mater. Chem. Phys.* **2004**, *88*, 192–196.
[73] Y. Shan, L. Gao, *Mater. Chem. Phys.* **2005**, *89*, 412–416

Received: June 8, 2005
Published Online: September 23, 2005

